Analytical Predictions and Lattice Boltzmann Simulations of Intrinsic Permeability for Mass Fractal Porous Media

Abdullah Cihan,* Michael C. Sukop, John S. Tyner, Edmund Perfect, and Haibo Huang

We derived two new expressions for the intrinsic permeability (k) of fractal porous media. The first approach, the probabilistic capillary connectivity (PCC) model, is based on evaluating the expected value of the cross-sectional area of pores connected along various flow paths in the direction in which the permeability is sought. The other model is a modified version of Marshall's probabilistic approach (MPA) applied to random cross matching of pores present on two parallel slices through a fractal porous medium. The Menger sponge is a three-dimensional mass fractal that represents the complicated pore space geometry of soil and rock. Predictions based on the analytical models were compared with estimates of k derived from lattice Boltzmann method (LBM) simulations of saturated flow in virtual representations of Menger sponges. Overall, the analytically predicted k values matched the k values from the LBM simulations with <14% error for the deterministic sponges simulated. While the PCC model can represent variation in permeability due to the randomization process for each realization of the sponge, the MPA approach can capture only the average permeability resulting from all possible random realizations. Theoretical and empirical analyses of the surface fractal dimension (D_2) for successive slices through a random Menger sponge show that the mean D_2 value $\langle D_2 \rangle = D_3 - 1$, where D_3 is the three-dimensional mass fractal dimension. Incorporating $\langle D_2 \rangle$ into the MPA approach resulted in a k that compared favorably with the modal value of k from LBM simulations performed on 100 random realizations of a random Menger sponge.

ABBREVIATIONS: LBM, lattice Boltzmann method; MPA, Marshall's probabilistic approach; PCC, probabilistic capillary connectivity.

A. Cihan and J.S. Tyner, Biosystems Engineering and Soil Science, Univ. of Tennessee, 2506 E.J. Chapman Dr., Knoxville, TN 37996-4531; M.C. Sukop and H. Huang, Dep. of Earth Sciences, Florida International Univ.; and E. Perfect, Dep. of Earth and Planetary Sciences, Univ. of Tennessee, Knoxville, TN, 37996-1410. A. Cihan now at Environmental Science and Engineering, Colorado School of Mines, Coolbaugh Hall 310, Golden, CO 80401-1887. Received 7 Jan. 2008. *Corresponding author (acihan@mines.edu).

SINCE THE INTRODUCTION OF FRACTALS as new geometric models for natural objects, numerous efforts have been made to harness their mathematics for solving outstanding problems in hydrology. Fractals are inherently scaling. Thus, with the current interest in upscaling hydraulic properties, fractal models are being reexamined as viable descriptors of soils, aquifers, and reservoir rocks. Several theoretical investigations of the intrinsic permeabilities of fractal porous media have been presented in the past few decades. These are discussed below as a preface to the derivation of two new analytical models based on probabilistic fractal approaches.

Early studies attempted to formulate expressions for permeability based on the Kozeny–Carman equation. The results suggested a general relationship between intrinsic permeability (k)

and porosity (ϕ) of the form $k \propto \phi^\lambda$, where λ is a scaling exponent. Different researchers found various expressions for the exponent λ as a function of the pore or mass fractal dimension (e.g., Jacquin and Adler, 1987; Muller and McCauley, 1992). Gimenez et al. (1997) reviewed this research and developed their own intrinsic permeability model incorporating the effects of tortuosity and connectivity into the exponent λ. The Kozeny–Carman equation was also analyzed by Xu and Yu (2008), who suggested a theoretical relationship for the Kozeny–Carman constant as a function of porosity, pore fractal dimension, and tortuosity.

Adler and Thovert (1993) performed extensive numerical experiments by solving the Navier–Stokes equations for flow in one-, two-, and three-dimensional fractal structures. Their results were consistent with a generalized Kozeny–Carman equation for one-dimensional flow in a "stretched" Sierpinski carpet. The scaling relationship between k and ϕ turned out to be unreliable, however, for two- and three-dimensional deterministic and random fractal porous media.

More recently, Yu and Liu (2004) developed a fractal model for k by assuming continuous fractal pore-size and pore-length distributions based on Poiseuille's equation. Xu et al. (2006a) developed tortuosity and permeability models for flow through a fractal-like tree network between one point and a straight line. The effective permeability of this network was obtained, both in parallel and in series, using Poiseuille's equation including the effect of tortuosity. Xu et al. (2006b) extended this approach to find the permeability of a fractal disk-shaped network.

Following a different line of attack, Hunt (2001) used continuum percolation theory to find the volume fraction of

continuously distributed pores whose sizes are greater than or equal to a critical pore radius. The critical value, or the smallest pore in a connected network, was then related to the permeability based on an analogy between the Poiseuille and Darcy equations. This analysis, like most of those discussed above, assumes all of the pores are interconnected. It does not take into account the possibility of disconnected pores, which do not contribute to flow. Since disconnected pores can occur in natural porous media, the ability of such fully connected fractal models to accurately predict the k of real soils and rocks is not clear.

Rawls et al. (1993) attempted to deal with the issue of disconnected pores by combining Marshall's (1958) probabilistic approach with the fractal properties of a Sierpinski carpet. In the Marshall (1958) model, two surfaces, each of which consists of n sections, are exposed along a cut through an isotropic porous medium and then rejoined randomly. The surfaces are connected through necks, which are assumed to be equal in size to the smallest mean pore area between any two contacting pores. Each n section is assumed to have the same fraction of pore area, which is defined as the areal porosity. The n classes of pore cross-sections are denoted by a sequence of mean radii as r_1, r_2, …, r_n. The average area of the pore necks is then calculated and related to k:

$$k = C \frac{\phi^a}{n^2} \sum_{i=1}^{l} 2(l-i) r_i^2 \qquad [1]$$

where C is a constant that depends on the pore geometry, l is the number of pore classes up to n, and a is a correction factor introduced later by Millington and Quirk (1961). In Marshall's (1958) original study, $a = 2$. Rawls et al. (1993) modified Eq. [1] for fractal structures by replacing r_i with r_0/b^i and obtained

$$k = C \phi^a \frac{r_1^2}{n^2} \qquad [2]$$

where r_0 is the width of the Sierpinski carpet, b is the scaling factor, and r_1 is the largest equivalent pore radius. Equation [2] assumes that each pore size r_i has the same fractional area; however, this is not realistic for a fractal structure. When two surfaces from a cross-section through a fractal porous medium are rejoined randomly, as in the original Marshall approach, there will be different pore sizes with different fractional areas, as opposed to the assumption of a constant fraction of pores. Thus, statistically matching two randomized fractal carpet surfaces will result in a different formulation from Eq. [2].

In this study, we developed two new analytical expressions for the intrinsic (saturated) permeability by using probabilistic and fractal methods based on the connectivity of pores and Marshall's (1958) approach. We tested these models using LBM simulations performed in well-defined, explicit fractal structures (i.e., deterministic and random Menger sponges). The LBM simulations were utilized to validate our analytical models because construction of actual Menger sponges is extremely difficult (Kirihara et al., 2006; Mayama and Tsujii, 2006) and, as a result, no experimental studies of their hydraulic properties have been reported to date.

Physical Properties of Deterministic and Randomized Menger Sponges

The Menger sponge is a three-dimensional mass fractal with the capability of simulating a wide range of pore sizes and configurations. It is named after the mathematician Karl Menger (Mandelbrot, 1982). The Menger sponge fractal has long been used as a model substrate for simulating flow and transport problems in complex pore space geometries (e.g., Garrison et al., 1992; Garza-López et al., 2000; Cihan et al., 2007).

The Menger sponge is constructed from a solid *initiator* cube (embedding dimension $E = 3$) of unit length by an iterative process of mass removal and rescaling. A *generator* is defined by subdividing the initiator into $b^E = 27$ smaller cubes of length $l = 1/b = 1/3$, and removing $m = 7$ of these. In the classical (deterministic) Menger sponge, six of the removed cubes are central to the six faces of the initiator, while the remaining removed cube comes from the center of the initiator (Fig. 1a). In a random Menger sponge, the seven removed cubes are randomly chosen from the 27 solid cubes of length $1/b$ (Fig. 1b). Construction continues by repeatedly applying the generator to the remaining solid cubes. Note that l depends on b and i as $l_i = 1/b^i$, where $i = 1, 2, 3, …$ is the level of iteration of the fractal algorithm. The number of solid cubes of length l_i, $N_{s3}(l_i)$, at the first iteration is $N_{s3}(1/3) = 20$. At the second iteration $N_{s3}(1/9) = 400$, and so on. In general, we have $N_{sE}(1/b^i) = b^{iD_E}$ where D_E is the mass fractal dimension defined by the ratio $\log(b^E - m)/\log(b)$, with m being the number of cubes removed in the generator. The number of pores, N_{pE}, of length l is given by

$$N_{pE}^{(i)} = n_p b^{(i-1)D_E} = \left(b^E - b^{D_E}\right) b^{(i-1)D_E} \qquad [3]$$

where n_p is the number of pores in the generator, which is equal to $m = 7$ for the Menger sponge. The porosity at any iteration level, n, is formulated by
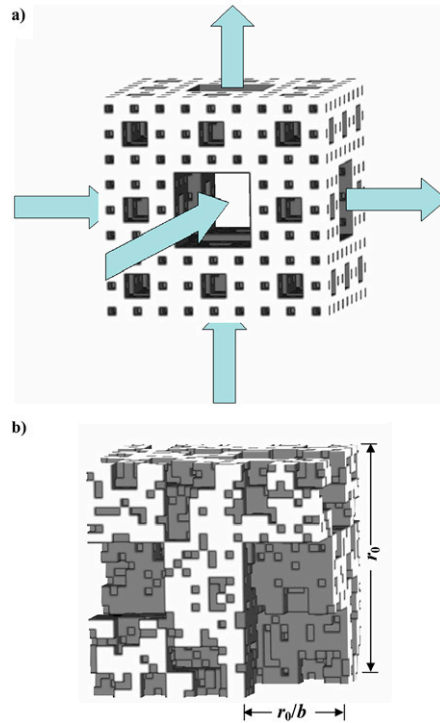

FIG. 1. (a) Deterministic Menger sponge of unit width and scaling factor $b = 3$, last iteration level $n = 3$, a mass fractal dimension of D_3 = log20/log3 = 2.726… and D_2 = log8/log3 = 1.892… for each face of the cube, and (b) one realization of a randomized Menger sponge with unit width and $b = 3$, $n = 3$, $D_3 = 2.726$, and $\langle D_2 \rangle = 1.726$ (r_0 is the width of the Menger sponge).

$$\phi_E = \sum_{i=1}^{n} \frac{N_p^{(i)}}{b^{iE}} = 1 - b^{n(D_E - E)} \tag{4}$$

where $E = 3$ for the volumetric porosity of the Menger sponge.

Figure 1 shows a deterministic Menger sponge and an example realization of a random Menger sponge iterated up to $n = 3$ with $b = 3$ and $D_3 = 2.726\ldots$. The surface fractal dimensions (D_2) of both structures change with distance (or slice number = b^i) moving from one face through the interior to the opposite face. Figure 2 shows the variation in D_2 as a function of slice number for both deterministic and random Menger sponges. The maximum value of D_2 inside the deterministic Menger sponge is $1.892\ldots$, which is the fractal dimension of the Sierpinski carpet; the minimum value of $D_2 = 1.261\ldots$ occurs in the middle of the deterministic sponge.

Surface fractal dimensions of the slices inside a randomized Menger sponge change for each realization of the sponge due to the randomization process. Figure 2 shows changes in D_2 with slice number for one example realization of a random Menger sponge. Figure 2 also shows changes in the mean value of D_2 for each slice based on 100 random realizations. The line is almost invariant and indicates that $\langle D_2 \rangle \sim D_3 - 1$, where $\langle D_2 \rangle$ is the mean value. A formal proof of this result is given below.

For the sake of simplicity, we will only consider the first iteration level, since it will be sufficient to deduce information about the relationship between $\langle D_2 \rangle$ and D_3. At $i = 1$, the number of boxes (either solid or pore), $n_b^{(1)}$, in each slice is equal to b^2. The number of solids inside the Menger sponge generator as a whole is given by b^{D_3}, while the probability or proportion of $1/b^1$ sized solids, p_1, in the whole system is b^{D_3}/b^3. The probability of obtaining x_1 number of $1/b^1$ sized solids from a random slice with b^2 boxes through this structure when sampling without replacement can be calculated from the hypergeometric distribution. The expected value of x_1 from the hypergeometric distribution is given by $\langle x_1 \rangle = n_b^{(1)} p_1 = b^{(D_3 - 1)}$. Then, by definition, the mean surface fractal dimension of multiple slices through a single randomized Menger sponge (or single slices through multiple random realizations) must be

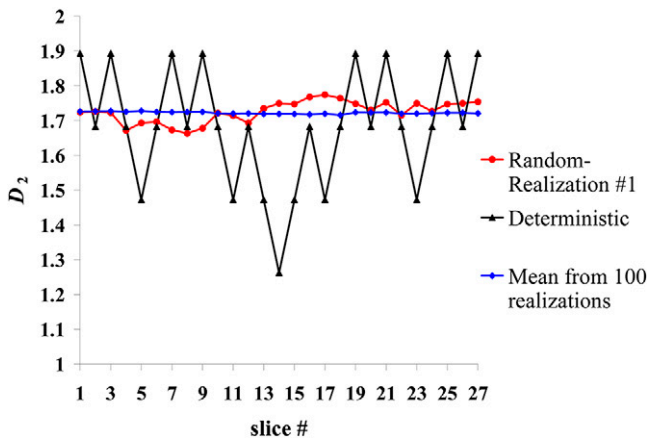$$\langle D_2 \rangle = \frac{\log \langle x_1 \rangle}{\log b} = D_3 - 1 \tag{5}$$

FIG. 2. Variation of the fractal dimension D_2 through slices of deterministic and random Menger sponges with scaling factor $b = 3$, last iteration level $n = 3$, and fractal dimension $D_3 = 2.726$.

which explains the observed behavior in Fig. 2. According to the definition of porosity given by Eq. [4], Fig. 2 and Eq. [5] imply that $\langle \phi_2 \rangle = \phi_3$, i.e., the mean areal porosity is equal to the volumetric porosity. This is a convenient assumption commonly used in subsurface hydrology.

The scaling factor b represents the length ratio of the initiator relative to the largest pore present, and thus could be estimated from sample dimensions and water retention data. If the characteristic size is chosen as the length of a sampled soil, b can be calculated from the ratio of the sample size to the maximum pore size or minimum capillary pressure ("air entry value" in length units). Finer textured or clay-rich soils can be expected to exhibit larger b values than coarser soils for a constant characteristic size (Brakensiek and Rawls, 1992).

Gibson et al. (2006) reported independent estimates of b and D_E for soil aggregates based on image analysis and density scaling of two- and three-dimensional computed tomographic scans. The values of b and D_3 ranged from 4 to 15 and from 2.97 to 2.99, respectively. Their results also indicate that $\langle D_2 \rangle \sim D_3 - 1$.

Analytical Models for Intrinsic Permeability

Neglecting inertial effects, the mean velocity of a fluid, u, in a narrow tube of radius r_t is given by the Poiseuille equation:

$$u = -\frac{Cr_t^2}{\mu}\frac{d\psi}{dl} \tag{6}$$

where C is a shape factor, μ is the dynamic viscosity (Pa s), and $d\psi/dl$ is the pressure gradient driving the fluid flow in the tube. If the porous medium is considered to be made up of channels of different sizes, Poiseuille's equation is analogous to Darcy's law, which expresses the mean velocity of a fluid in a porous medium, and can be written as

$$q = -\frac{k}{\mu}\frac{d\psi}{dl} \tag{7}$$

where k is equivalent to $\langle Cr_t^2 \rangle$, which is an averaged quantity for a porous medium. The shape factor C changes depending on the geometry of the pore. Its value is equal to 1/8 for circular pores. Pores in the Menger sponge are square, however, and flow is assumed to be in the z direction. Neglecting inertial and end effects, and assuming no interaction between adjacent pores (pores are assumed to be surrounded with solid boundaries where a no-slip boundary condition applies at the walls of a square), the solution of the Navier–Stokes equation for the average velocity within an individual square pore is given by (Papanastasiou et al., 2000)

$$u_i = -C\frac{d_i^2}{\mu}\frac{d\psi}{dz}$$

$$C = \frac{1}{12}\left[1 - 6\sum_{k=0}^{\infty}\frac{\tanh[\pi(k-1/2)]}{\pi^5(k-1/2)^5}\right] \sim 0.035 \tag{8}$$

where d is the side length of the pore. The area of pores at the ith iteration level of the Menger sponge algorithm can be written as $d_i^2 = r_0^2/b^{2i}$ where r_0 is the width of the sponge.

Probabilistic Capillary Connectivity Model

The method used here separates the system into different connected flow paths or networks. Consider a network consisting

of only the largest pores of size r_0/b connected from one end to the other in the direction of flow. According to Poiseuille's equation, the mean velocity of water following such a pathway is proportional to r_0^2/b^2. We define a probability for the existence of such a network as $P_1 N_{p3}^{(1)}/b^3$, where $N_{p3}^{(1)}/b^3$ is the proportion of the largest pores in the whole volume and P_1 represents the proportion of pores of size r_0/b connected from one end to the other. The remaining proportion of pores of size r_0/b is given by $(1-P_1)N_{p3}^{(1)}/b^3$; these pores may be completely unconnected or connected with smaller pores of size r_0/b^2 to form a different flow pathway. There might also be a network formed by only the r_0/b^2 sized pores. The probability for the existence of a network containing r_0/b^2 sized pores or r_0/b and r_0/b^2 sized pores is written as $P_2(N_{p3}^{(2)}/b^{2\times3} + (1-P_1)N_{p3}^{(1)}/b^3$, where P_2 represents the connected proportion of pores in networks formed by r_0/b^2 or larger sized pores. Since flow is controlled by the smallest pores within a network of different-sized pores connected in series, the mean velocity of water following a pathway consisting of r_0/b and r_0/b^2 sized pores is assumed to be proportional to the area of the smaller pores, i.e., r_0/b^2. In generalized form, the pore areas controlling flow in the different flow paths, multiplied by their associated probabilities, are written as

$$i=1 \quad P_1 \frac{N_{pE}^{(1)}}{b^E} \frac{r_0^2}{b^2}$$

$$i=2 \quad P_2\left[\frac{N_{pE}^{(2)}}{b^{2E}}+(1-P_1)\frac{N_{pE}^{(1)}}{b^E}\right]\frac{r_0^2}{b^4}$$

$$i=3 \quad P_3\left[\frac{N_{pE}^{(3)}}{b^{3E}}+(1-P_2)\frac{N_{pE}^{(2)}}{b^{2E}}+(1-P_2)(1-P_1)\frac{N_{pE}^{(1)}}{b^E}\right]\frac{r_0^2}{b^6} \quad [9]$$

$$\vdots \qquad \vdots$$

$$i=n \quad P_n\left[\frac{N_{pE}^{(n)}}{b^{nE}}+(1-P_{n-1})\frac{N_{pE}^{(n-1)}}{b^{(n-1)E}}+\cdots\right.$$
$$\left.+(1-P_{n-1})(1-P_{n-2})\ldots(1-P_1)\frac{N_{pE}^{(1)}}{b^E}\right]\frac{r_0^2}{b^{2n}}$$

Permeability is defined by the expected value, $\langle Cr_t^2\rangle$, i.e., the summation of all the terms above leading to

$$k(n)=Cr_0^2\sum_{i=1}^{n}\sum_{j=i}^{n}\frac{N_{pE}^{(i)}}{b^{iE}}\frac{P_j}{b^{2j}}\prod_{k=i}^{j-1}(1-P_k) \qquad [10]$$

where n is the last iteration level of the fractal porous medium, and the pore shape factor C is assumed to be constant for all pores. Summation of the probabilities yields the connected proportion of pores in the flow system and is equivalent to the effective porosity, $\phi_{\text{eff }E}$:

$$\phi_{\text{eff }E}(n)=\sum_{i=1}^{n}\sum_{j=i}^{n}\frac{N_{pE}^{(i)}}{b^{iE}}P_j\prod_{k=i}^{j-1}(1-P_k) \qquad [11]$$

Cihan et al. (2007) used a similar approach in their analysis of scale-variant fractal water retention functions during monotonic drainage. The different P_i values in Cihan et al. (2007) indicated the connected proportions of water-filled pores at different

suction levels and were named the *probability of drainage*. Here, since all the pores are filled with water, each P_i value represents the proportion of connected pores whose sizes are $\geq 1/b^i$. When $P_i \to 1$, the system approximates a "stretched" Sierpinski carpet. Now if we consider a steady flow field created in a deterministic Menger sponge by a pressure gradient in one direction (constant-pressure boundary conditions are applied on two opposing faces and the rest are assigned to be no-flow boundary conditions), the proportion of the largest pores of size r_0/b connected from one end to the other in the direction of the flow, P_1, is 3/7. The same statistics apply for r_0/b^2 sized pores connected from one end to the other in the direction of the flow because 3/7 of these pores are connected to the remaining 4/7 of the r_0/b sized pores, i.e., $P_2 = P_1 = 3/7$.

Assuming that all of the probabilities are constant and equal, i.e., $P = P_1 = P_2 = \ldots = P_n$, evaluation of the series for $E = 3$ in Eq. [10] and [11] renders

$$k(n)=Cr_0^2\frac{P\left(b^3-b^{D_3}\right)}{P-1+b^2}\left[\frac{(1-P)^{\frac{\log(1-\phi_3)}{(D_3-3)\log b}}-(1-\phi_3)}{b^{D_3}+b^3(P-1)}\right.$$
$$\left.\frac{(1-P)}{(1-\phi_3)^{2/(D_3-3)}}+b^2\frac{1-(1-\phi_3)^{\frac{D_3-5}{D_3-3}}}{b^5-b^{D_3}}\right] \qquad [12]$$

$$\phi_{\text{eff}3}(n)=$$
$$\phi_3-\frac{\left(b^3-b^{D_3}\right)(1-P)}{b^{D_3}+b^3(P-1)}\left[-(1-P)^{\frac{\log(1-\phi_3)}{(D_3-3)\log b}}+(1-\phi_3)\right] \qquad [13]$$

where $\phi_3 = 1-(b^n)^{D_3-3}$ is the total porosity. Since the P values in Eq. [10–13] are allowed to vary with direction, the above expressions can also be written in tensor form for applications in anisotropic systems.

Variation of the effective porosity with the total porosity for various P values is presented in Fig. 3. In this and the following figures, the x and y axes are labeled in terms of generic length units that can be equated to any unit system (centimeters, meters, etc.) depending on the units of the characteristic size chosen. Figure 3 shows that as the connectivity of the system measured
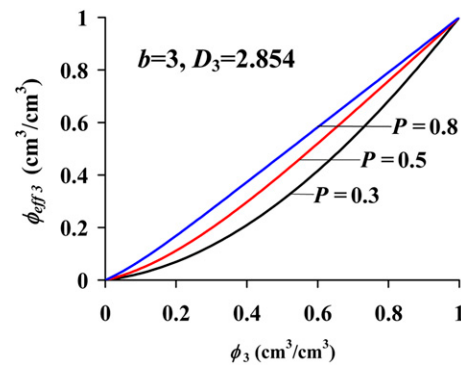

FIG. 3. Variation of effective porosity ($\phi_{\text{eff }3}$) with total porosity (ϕ_3) as a function of the measure of connectivity (P) for the probabilistic capillary connectivity model with scaling factor $b = 3$ and fractal dimension $D_3 = 2.854$ (characteristic size $r_0 = 1$ cm, pore shape factor $C = 0.035$).

with P decreases, the effective porosity decreases compared with the total porosity. In Fig. 3, b and D_3 were kept constant while n was varied. Varying only the iteration level n means that pores formed at previous iteration levels $<n$ are kept without changing their sizes while new smaller and smaller pores are added as n increases. Thus, the permeability approaches a limit beyond which it no longer changes with n because the contribution of infinitely small pores to flow is negligible compared with larger pores. As n approaches infinity, Eq. [12] reduces to

$$k = Cr_0^2 \frac{Pb^2\left(b^3 - b^{D_3}\right)}{\left(P - 1 + b^2\right)\left(b^5 - b^{D_3}\right)} \qquad [14]$$

Figure 4a presents changes in the permeability as a function of b for various P values when n = 3 and D_3 = 2.726… . As stated above, P is a measure of connectivity. When P = 0, the system is below the percolation threshold, and the permeability is zero. As P increases, the permeability increases as a result of increasing connectivity among pores (Fig. 4a). Intersection of the permeability curves with the vertical dashed line at b = 3 in Fig. 4a corresponds to three possible values of the permeability for a random Menger sponge whose properties were reviewed above. Figure 4a clearly indicates the ability of the PCC model to represent variation in k due to randomization.

Another way to analyze the permeability is to plot its variation with different values of D_3 (Fig. 4b). The permeability initially increases starting from zero as b increases because large pores form in an initially solid system with zero porosity. Increasing the scaling factor increases the number and decreases

the size of the pores as porosity increases. As a result, the permeability curves exhibit well-defined maxima in Fig. 4b. Beyond the maximum, permeability begins to decrease because the flow rate is less in a system having smaller pore sizes due to greater b values despite increasing porosity. This behavior resembles the phenomenon that we observe in natural soils (e.g., clay generally has much more porosity than sand, but it is much less permeable). Figure 4b also shows that the permeability maximum decreases with increasing mass fractal dimension, which typically increases with increasing clay content (Filgueira et al., 2006).

From the above discussion, a P value of 3/7 can be used in Eq. [12] and [14] for the prediction of the intrinsic permeability of a deterministic Menger sponge. Since the P values are not necessarily equal in a random Menger sponge, forward prediction by applying Eq. [12] or [14] to random structures may not be possible. For such structures, P is assumed to be a constant effective parameter, equivalent to a measure of connectivity that can be estimated inversely by comparison with experimental or numerical simulation results. For forward prediction of intrinsic permeability in the case of random Menger sponges, Marshall's probabilistic approach can be followed.

Marshall's Probabilistic Approach

Following an approach similar to Marshall (1958), two surfaces from a cross-sectional cut through a random Menger sponge are rejoined randomly (Fig. 5). The surfaces are connected through pore necks, whose sizes are assumed to be the intersection areas between pairs of contacting pores. Table 1 shows an example of the calculation of probabilities of possible pore neck areas that result from matching two randomized unit fractal faces at the second iteration level. Each fractal face has the same fractal dimension, D_2 = log7/log3. The width of the largest pores is 1/3 and the areal fraction of the largest pores is 2/9. The width of the smallest pores with areal fraction of 14/81 is $1/3^2$ (Table 1). Matching these two faces may result in two possible pore neck areas. One possibility for any given realization of the faces is that the largest pores on one face can match with those on the other face, which results in a pore neck area of $1/3^2$. The other possibility is the $1/3^4$ pore neck area that might result from intersecting a 1/3 with a $1/3^2$ pore or a $1/3^2$ with a $1/3^2$ pore width on one face with the other. Since the randomization of the faces associated with the same fractal dimension are assumed to be independent events, the probability of a $1/3^2$ pore neck area can be calculated by multiplying the areal fraction of pores of 1/3 width in the two faces, i.e., $p(1/3^2) \cap p(1/3^2)$ = 2/9 × 2/9 =
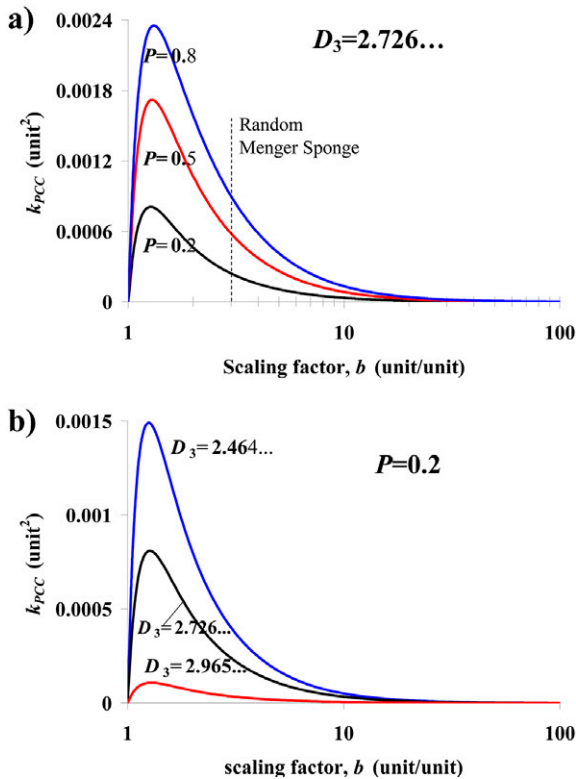
FIG. 4. Variation of the probabilistic capillary connectivity (PCC) model intrinsic permeability (k) with the model parameters: (a) k_{PCC} vs. scaling factor b as a function of the measure of connectivity P when the fractal dimension D_3 = 2.726… and (b) k_{PCC} vs. b as a function of D_3 when P = 0.2 (characteristic size r_0 = 1 cm, pore shape factor C = 0.035).
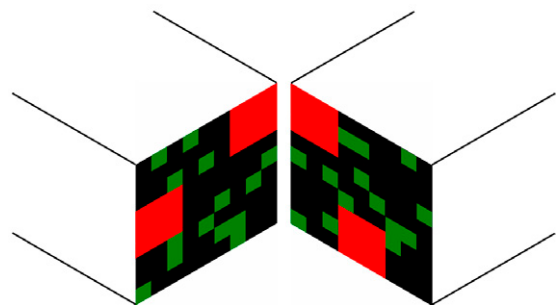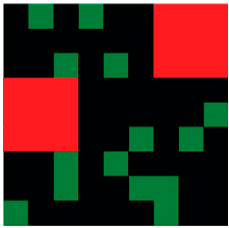
FIG. 5. Matching of two random fractal surfaces of the same scaling factor b and fractal dimension D_2 values (adapted from Hillel, 1998).

TABLE 1. Example calculation of probability of neck areas resulting from matching of two randomized faces with unit width. In the first row, only the pores shaded with red are taken into account to calculate the probability of the neck area in the third column. In the second row, the green phase indicates the pores contributing to the calculation of the probability of the neck area at the next level.

Face 1	Face 2	Probable neck area	Probability
$p(1/3^2) = 2/9$†	$p(1/3^2) = 2/9$	$1/3^2$	$p(1/3^2) \cap p(1/3^2) = 2/9 \times 2/9 = 4/81$
$p(1/3^4) = 14/81$	$p(1/3^4) = 14/91$	$1/3^4$	$p(1/3^4) \cap p(1/3^4) + p(1/3^2) \cap p(1/3^4) + p(1/3^4) \cap p(1/3^2) = (14/81)^2 + 2(14/81)(2/9) = 700/(81)^2$

† $p()$ indicates areal proportion of pores.

4/81. Likewise, the probability of a $1/3^4$ pore neck area can be calculated by taking into account all possible pore pairs that give $1/3^4$ neck area, i.e., $p(1/3^4) \cap p(1/3^4) + 2[p(1/3^2) \cap p(1/3^4)]$. The second term is multiplied by two because as the pores of $1/3$ width in the first face may intersect with the pores of $1/3^2$ width in the second face, the pores of $1/3$ width present in the second face may also intersect with the pores of $1/3^2$ width in the first face, which result in a $1/3^4$ pore neck area.

Generalization of the above procedures to matching of any arbitrary two faces with the same arbitrary fractal dimension is as follows. The areal fraction of pores of size $1/b$ is equal to $p(1/b^2) = N_{p2}^{(1)}/b^2$, where $N_{p2}^{(1)}$ is the number of pores generated at the first iteration level of a slice ($E = 2$) in a fractal porous medium. The probability of occurrence for the solid space area is equal to $1 - \phi_2^2$. The probability of occurrence of $1/b^2$ neck areas resulting from the intersection of pores with $1/b$ width on one surface with pores of $1/b$ width on the other surface can be evaluated as $p(1/b^2) \cap p(1/b^2) = [N_{p2}^{(1)}/b^2]^2$. Likewise, the probability of occurrence of $(1/b^2)^2$ neck areas resulting from the intersection of pairs of pores $1/b^2$–$1/b^2$ and $1/b$–$1/b^2$ on the matching surfaces can be written as $[N_{p2}^{(2)}/b^4]^2 + 2[N_{p2}^{(2)}/b^2 \times N_{p2}^{(2)}/b^4]$. The probabilities for all possible neck areas are given in Table 2.

According to the axiom of probability, summation of the probabilities must equal unity:

TABLE 2. Neck area vs. probability from the random intersection of two fractal surfaces.

Probable pore neck area†	Probability‡
0	$1 - \phi^2$
$(1/b)^2$	$(N_p^{i=1}/b^2)^2$
$(1/b^2)^2$	$(N_p^{i=2}/b^4)^2 + 2[(N_p^{i=1}/b^2)((N_p^{i=1}/b^4)]$
$(1/b^3)^2$	$N_p^{i=3}/b^6 + 2[(N_p^{i=1}/b^2)(N_p^{i=3}/b^6)] + 2[(N_p^{i=2}/b^4)(N_p^{i=3}/b^6)]$
⋮	⋮

† b is a scaling factor.
‡ N_p is the number of pore elements, i is the iteration level.

$$\sum p_i =$$
$$1 - \phi_2^2 + \left[\sum_{i=1}^{n} \sum_{j=i}^{n} \frac{N_{p2}^{(i)}}{b^{2i}} \frac{N_{p2}^{(j)}}{b^{2j}} + \sum_{i=2}^{n} \sum_{j=1}^{i-1} \frac{N_{p2}^{(i)}}{b^{2i}} \frac{N_{p2}^{(j)}}{b^{2j}} \right] = 1 \quad [15]$$

The term in the brackets of Eq. [15] is a symbolic representation for the summation of the probabilities in Table 1 excluding the probability of the zero neck area, $1 - \phi_2^2$. The term in the brackets can be shown to be equal to $[1 - b^{i(D_2-2)}]^2 = \phi_2^2$ by evaluating the series after substitution of $N_{p2}^{(i)} = (b^2 - b^{D_2}) b^{D_2(i-1)}$. Multiplying probable neck areas with the probabilities and summing across all sizes, we obtain the total expected area, $\langle r_t^2 \rangle$, which can be written in symbolic form as

$$\langle r_t^2 \rangle =$$
$$r_0^2 \left[\sum_{i=1}^{n} \sum_{j=i}^{n} \frac{N_{p2}^{(i)}}{b^{2i}} \frac{N_{p2}^{(j)}}{b^{2j}} \left(\frac{1}{b^j}\right)^2 + \sum_{i=2}^{n} \sum_{j=1}^{i-1} \frac{N_{p2}^{(i)}}{b^{2i}} \frac{N_{p2}^{(j)}}{b^{2j}} \left(\frac{1}{b^i}\right)^2 \right] \quad [16]$$

where r_0 is the characteristic length of the porous medium that shows fractal behavior. Recalling the definition of k previously given and invoking the relationship $\langle D_2 \rangle = D_3 - 1$, we can formulate the permeability of a random Menger sponge by evaluating the series in Eq. [16] as

$$k(n) = C r_0^2 \left[\frac{\left(b^2 - b^{\langle D_2 \rangle}\right)^2 \left(b^4 + b^{\langle D_2 \rangle}\right)}{\left(b^4 - b^{\langle D_2 \rangle}\right)\left(b^6 - b^{2\langle D_2 \rangle}\right)} \right.$$
$$- 2 \frac{\left(b^2 - b^{\langle D_2 \rangle}\right)}{\left(b^4 - b^{\langle D_2 \rangle}\right)} \left(1 - \langle \phi_2 \rangle\right)^{\frac{\langle D_2 \rangle - 4}{\langle D_2 \rangle - 2}}$$
$$\left. + \frac{\left(b^4 - b^{2\langle D_2 \rangle}\right)}{\left(b^6 - b^{2\langle D_2 \rangle}\right)} \left(1 - \langle \phi_2 \rangle\right)^{\frac{2\langle D_2 \rangle - 6}{\langle D_2 \rangle - 2}} \right] \quad [17]$$

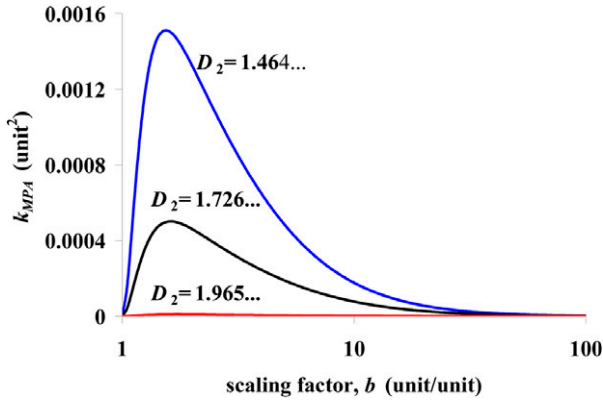where $\langle \phi_2 \rangle = 1 - (b^n)^{\langle D_2 \rangle - 2}$.

FIG. 6. Variation of Marshall's probabilistic approach intrinsic permeability (k_{MPA}) with scaling factor b as a function of fractal dimension D_2 (characteristic size r_0 = 1 cm, pore shape factor C = 0.035).

The variation of k with b predicted by Eq. [17] is shown in Fig. 6. The MPA model shows a very similar behavior to the PCC model for the different values of $\langle D_2 \rangle$. Application of the MPA model is limited to more or less isotropic porous media since the mean surface fractal dimension $\langle D_2 \rangle$ is representative for the whole structure, while the variation of k along different directions in anisotropic systems can only be taken into account by the PCC model.

Except for very low values of b, the series converges very quickly. Equation [17] can then be simplified by allowing $n \to \infty$:

$$k = C\,r_0^2\,\frac{\left(b^2 - b^{\langle D_2 \rangle}\right)^2\left(b^4 + b^{\langle D_2 \rangle}\right)}{\left(b^4 - b^{\langle D_2 \rangle}\right)\left(b^6 - b^{2\langle D_2 \rangle}\right)} \qquad [18]$$

The Lattice Boltzmann Method

Detailed introductions to the LBM can be found in Sukop and Thorne (2006), Succi (2001), and Wolf-Gladrow (2000). Here we provide a brief summary of the three-dimensional LBM applied to numerically compute the permeability of the deterministic and random Menger sponges. This single-phase fluid flow problem is among the simplest capabilities of the LBM and the current work can be viewed as a prelude to future efforts that will consider unsaturated flows. We used the simplest Bhatnagar–Gross–Krook (BGK) single relaxation time model in this study. The BGK model is known to have limitations (Pan et al., 2006), but careful application gives adequate results in many applications.

We have implemented the LBM in three dimensions for a single-component system. The distribution function f represents a fluid and satisfies the following lattice Boltzmann equation:

$$f_a\left(\mathbf{x} + \mathbf{e}_a\Delta t, t + \Delta t\right) =$$
$$f_a\left(\mathbf{x},t\right) - \frac{\Delta t}{\tau}\left[f_a\left(\mathbf{x},t\right) - f_a^{\mathrm{eq}}\left(\mathbf{x},t\right)\right] \qquad [19]$$

where $f_a(\mathbf{x},t)$ is the density distribution function in the ath velocity direction, τ is a relaxation time that is related to the kinematic viscosity through $\nu = c_s^2(\tau - 0.5\Delta t)$, and $\mathbf{e}_a$ is the discrete velocity. The equilibrium distribution function $f_a^{\mathrm{eq}}(\mathbf{x},t)$ can be calculated as

$$f_a^{\mathrm{eq}}\left(\mathbf{x},t\right) = w_a\rho\left[1 + \frac{\mathbf{e}_a\mathbf{u}}{c_s^2} + \frac{\left(\mathbf{e}_a\mathbf{u}\right)^2}{2c_s^4} - \frac{\mathbf{u}^2}{2c_s^2}\right] \qquad [20]$$

where ρ is the density of the fluid, which can be obtained from $\rho = \sum_{a=0}^{18} f_a$, $\mathbf{u}$ is the velocity of fluid, and w_a is the direction-specific weight. For the D3Q19 model, the discrete velocities are given by

$$\left[\mathbf{e}_0,\mathbf{e}_1,\mathbf{e}_2,\mathbf{e}_3,\mathbf{e}_4,\mathbf{e}_5,\mathbf{e}_6,\mathbf{e}_7,\mathbf{e}_8,\mathbf{e}_9,\mathbf{e}_{10},\mathbf{e}_{11},\mathbf{e}_{12},\mathbf{e}_{13},\mathbf{e}_{14},\mathbf{e}_{15},\mathbf{e}_{16},\mathbf{e}_{17},\mathbf{e}_{18}\right] =$$

$$c\begin{bmatrix} 0 & 1 & -1 & 0 & 0 & 0 & 0 & 1 & 1 & -1 & -1 & 1 & -1 & 1 & -1 & 0 & 0 & 0 & 0 \\ 0 & 0 & 0 & 1 & -1 & 0 & 0 & 1 & -1 & 1 & -1 & 0 & 0 & 0 & 0 & 1 & 1 & -1 & -1 \\ 0 & 0 & 0 & 0 & 0 & 1 & -1 & 0 & 0 & 0 & 0 & 1 & 1 & -1 & -1 & 1 & -1 & 1 & -1 \end{bmatrix}$$

w_a = 1/3 (a = 0), w_a = 1/18 (a = 1, 2, …, 6), w_a = 1/36 (a = 7, 8, …, 18), and $c_s = c/\sqrt{3}$, where $c_s = \Delta x/\Delta t$ is the ratio of lattice spacing Δx and time step Δt. Here, we define one lattice unit (Δx) as 1 lu. The macroscopic momentum $\rho\mathbf{u}$ is defined as

$$\sum_{a=0}^{18} f_a\mathbf{e}_a = \rho\mathbf{u} \qquad [21]$$

Pressure is proportional to density in this model and the relationship, known as the Equation of State, is $\Psi = c_s^2\rho$ or simply $\Psi = \rho/3$ for the model we use here.

Results and Discussion

Deterministic Menger Sponge

We calculated k as a function of the maximum iteration level (n) for a deterministic Menger sponge of 1-cm width with b = 3 and fractal dimension D_3 = 2.726 (Fig. 1a). Based on this information and setting P = 3/7, Eq. [12] was used to estimate k for unidirectional, steady, laminar flow of a fluid passing through the deterministic sponge. Because most of the flow is transmitted by the serially connected largest pores (Fig. 1a), which form at n = 1, there was not much difference between the k values estimated by the PCC model as a function of the maximum iteration level (Table 3). As discussed above, since the only changing variable is n, as n increases, the contribution of new smaller pores to the permeability becomes negligible compared with the larger pores already present. Going from n = 1 to n = 4, the intrinsic permeability increases by ~16%. The limiting form of the permeability given by Eq. [14] results in a k value differing by <0.15% from that given by Eq. [12] for the deterministic Menger sponge with n > 2. The pores present next to the side boundaries and the pores perpendicular to serially connected pores in

TABLE 3. Comparison of the results for intrinsic permeability (k) from the lattice Boltzmann method (LBM) and the probabilistic capillary connectivity (PCC) models for the deterministic Menger sponge.

Iteration level	Porosity, ϕ_3	Effective porosity, $\phi_{\mathrm{eff}\,3}$	k (PCC)	k (LBM)	Reynolds number (LBM)
			——— $\times 10^{-4}$ cm^2 ———		
1	0.26	0.11	4.34	5.02	0.36
2	0.45	0.26	4.97	5.53	0.39
3	0.59	0.40	5.04	5.66	0.40
4	0.70	0.53	5.05	5.73	0.41

the main flow direction do not contribute to flow significantly. Eliminating those pores, Eq. [13] can be defined as the effective porosity, which expresses the proportion of pores present in the main flow path. Table 3 shows the calculated values of effective porosity at different iteration levels. The ratio of the effective porosity to the total porosity varies between 0.42 and 0.76 from $n = 1$ to $n = 4$ (Table 3).

We also evaluated the intrinsic permeability of the deterministic Menger sponge illustrated in Fig. 1a using the LBM. We simulated flow at different levels of construction up to $n = 4$. The simulations used periodic boundaries on the sides of the domain (so the opposite sides were effectively connected) and pressure boundaries on the top and bottom that imposed a gradient across the fractal domain. The pressure distribution occurring across the sponge is shown from a slice of the simulation domain in a Menger sponge with $n = 3$ (Fig. 7). In a convenient form for the LBM, Darcy's law, Eq. [7], is

$$q = \frac{k}{\rho c_s^2 (\tau - 0.5) \Delta t} \frac{\Delta \psi}{L} \qquad [22]$$

where q is the Darcy flux (the average velocity of fluid exiting the entire face—including solid areas where the velocity is zero), $c_s^2(\tau - 0.5)$ is the kinematic viscosity, and $\Delta \Psi / L$ is the pressure gradient. Note that the average fluid density is used in the denominator of Eq. [22].

Here we provide a brief description of the calculation of intrinsic permeability and Reynolds numbers for the LBM measurements. For all cases in Table 3, the domain was 243 by 243 by 243 lu^3. Fluid densities of 1.005 and 0.995 mu lu^{-3} (mu is any appropriate mass unit that is compatible with all other variables) were applied to the ends of the model domains. This gives an average density of 1 mu lu^{-3} and corresponding inlet and outlet pressures of $\Psi_{in} = 0.335$ and $\Psi_{out} = 0.3316$ mu lu^{-1} s^{-2}, respectively. For the $i = 3$ sponge under those conditions, the observed flow through the system was about 16.25 lu^3 s^{-1}. The corresponding Darcy flux q is the flow divided by the cross-sectional area or $q = 16.25$ lu^3 $s^{-1}/(243 \times 243$ $lu^2) = 2.75 \times 10^{-4}$ lu s^{-1}. Solving Eq. [22] for permeability k, we get $k = 33.4$ lu^2. Conversion to

real units involves multiplication by the scale conversion factor as follows:

$$k(\text{physical}) = k(\text{LBM}) \left(\frac{L_{\text{physical}}}{L_{\text{LBM}}} \right)^2 \qquad [23]$$

where L_{physical} and L_{LBM} are the lengths of any comparable feature in physical and LBM units, respectively.

We computed the average Reynolds number as Re $= \bar{u} L / v$, where $\bar{u}$ is the mean pore velocity (q/ϕ_3), and v is the dynamic viscosity of water. The Reynolds number increased slightly with iteration level of the structure under a constant pressure gradient (Table 3), but it was low in all cases and flows were expected to be Darcian. When Re $= 0.40$ for a 1-cm sponge, the LBM k value for $i = 3$ is 5.66×10^{-4} cm^2, which compares very favorably to the PCC k value, 5.04×10^{-4} cm^2, predicted by our new analytical expression Eq. [12], which ignores inertial and end effects.

We also computed the permeability of the stretched Sierpinski carpet ($b = 3$, $D_2 + 1 = D_3 = \log24/\log3$, and $n = 3$) using both Eq. [12] and the LBM. Setting $P = 1$, Eq. [12] predicts a PCC k $= 4.81 \times 10^{-4}$ cm^2. The corresponding LBM k for the stretched Sierpinski carpet is 4.32×10^{-4} cm^2.

Random Menger Sponge

We computed k using the LBM for 100 realizations of the $b = 3$, $D = 2.726...$, and $n = 3$ randomized Menger sponge generated using the homogenous algorithm (Sukop et al., 2001). These are the same parameters that characterize the deterministic structure in Fig. 1a, the only difference being that the locations of the pores are allowed to vary randomly. Figure 1b shows one such realization. The distribution of the resulting permeability values is presented in Fig. 8, along with summary statistics. The distribution was strongly skewed toward the lower k values. The modal value of the LBM permeability for the random Menger sponge was 2.35×10^{-4} cm^2, which was approximately 54% lower than the permeability of the deterministic Menger sponge. The intrinsic permeability of the random structure calculated using the MPA model was also less than that of the deterministic Menger sponge (a 35% reduction in the case of $n = 3$). The k is reduced because the randomization process interrupts the direct flow paths through the largest pores, which increases the tortuosity and disconnects or isolates many pores from the main flow paths, which decreases the effective porosity.

Based on Eq. [17], and neglecting the effect of pore coalescence (i.e., assuming the shape factor, $C \sim 0.035$, does not change with the randomization), the MPA intrinsic permeability of a randomized Menger sponge of 1-cm width, with $b = 3$, $n = 3$, and a surface fractal dimension of $\langle D_2 \rangle = 1.726$, is predicted to be 3.27×10^{-4} cm^2. This value was closer to the mean value of k from the LBM simulations than the modal LBM k value, indicating a slight overestimation (Fig. 8). A quantitative comparison of the MPA
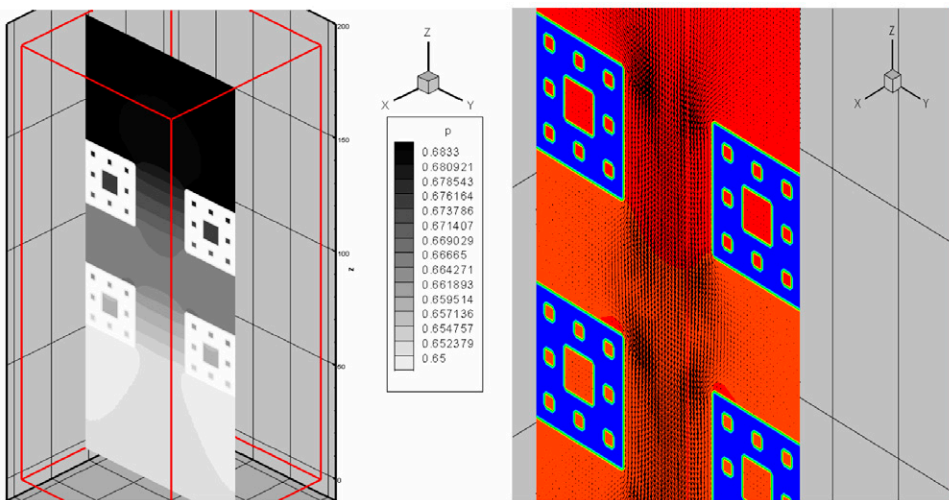

FIG. 7. Vertical slices through the center of a Menger sponge showing pressure distribution (left) and velocity vectors (right).
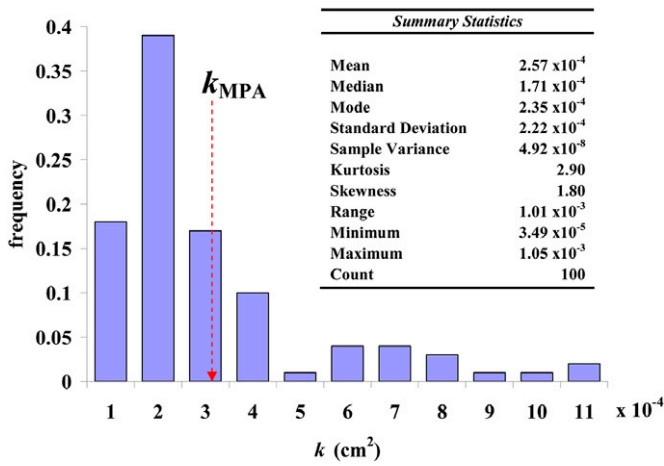
FIG. 8. Distribution of intrinsic permeability (k) from lattice Boltzmann method simulations in 100 realizations of the scaling factor b = 3, fractal dimension D = 2.726, and last iteration level n = 3 randomized Menger sponge.
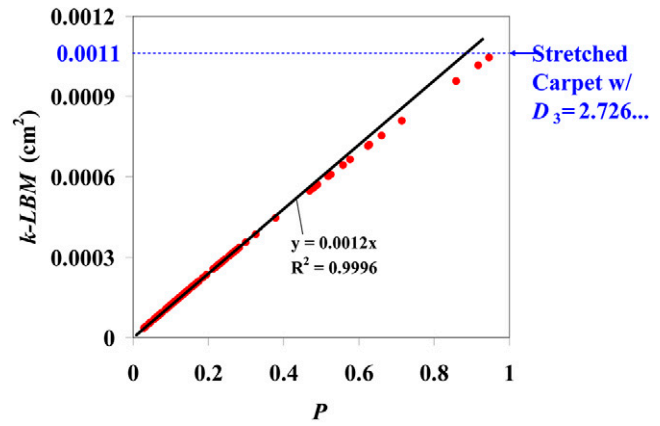

FIG. 9. Relationship between the measure of connectivity (P) and intrinsic permeability (k) from lattice Boltzmann method (LBM) simulations in 100 realizations of the scaling factor b = 3, fractal dimension D = 2.726, and last iteration level n = 3 randomized Menger sponge.

model results with the LBM simulations for the random Menger sponge is presented in Table 4.

The individual LBM k values were used to calculate a P value for each realization. The P values were inversely estimated from Eq. [12] by substituting the LBM k values. Figure 9 indicates a strong relationship between P and k. As expected, the value of P, the measure of connectivity, increases as the permeability increases. There is a linear relationship for $P \leq 0.4$; beyond that the relationship shows slight deviations from linearity. The dashed line indicates the permeability of a stretched carpet with P = 1. When the stretched carpet fractal dimension D_3 is equal to the dimension of the Menger sponge, i.e., 2.726… (D_2 = 1.726…), the PCC predicts a k value of approximately 1.1×10^{-3} cm². The modal P value in the PCC model was calculated to be 0.20 by equating Eq. [12] to the modal value of the LBM permeability from 100 realizations. This indicates that, on average, 20% of the pore volume, including the pores whose sizes are $\geq 1/b^i$ (i = 1, 2, and 3), can form a connected path from one end to the other. From Eq. [13] the mean effective porosity of the random Menger sponges at n = 3 was estimated as 0.23, compared with the total porosity of 0.594.

Conclusions

Applying Poiseuille's equation and probabilistic approaches, we obtained two new analytical expressions (PCC and MPA) to estimate the intrinsic (saturated) permeability of mass fractal porous media. While the PCC model is able to represent variation in permeability with a measure of connectivity due to the randomization process for each realization of the sponge, the MPA approach can capture only the average permeability resulting

from all possible random realizations. The application of the MPA permeability model may not be reliable in highly anisotropic and heterogeneous porous media due to high variation in D_2 along the direction in which k is measured. On the other hand, the PCC permeability model takes into account the anisotropy and heterogeneity, and also includes one additional variable (P) as a measure of connectivity.

The PCC model presented by Eq. [12] contains six physically based parameters (b, C, D_3, n, P, and r_0^2). Excluding P and replacing D_3 with $\langle D_2 \rangle$, the MPA model, Eq. [17], contains only five parameters. Although we have not tested any experimental procedures for applying these models to predict the intrinsic permeability of natural porous media in this research, we suggest the following methods for estimating the model parameters. The mass fractal dimension, D_3, can be estimated from fractal measurement methods such as voxel counting performed on three-dimensional computed tomographic scans of natural porous media. The mean surface fractal dimension, $\langle D_2 \rangle$, can be obtained by performing similar analyses on replicated digitized images of soil thin sections. The value of the scaling factor (b) is dependent on the characteristic length of the medium. If the characteristic length is chosen to be the size of the sample, as suggested in the literature, b can be calculated from the ratio of the sample size to the maximum pore size corresponding to the air-entry value. Once b is established, the iteration level (n) can be calculated from the ratio of the sample size to the minimum discernible pore size. If the iteration level of the medium is assumed to be large, then the limiting forms of the models (Eq. [14] and [18]) can be used, which eliminates one parameter, i.e., the iteration level. It is possible to estimate the P parameter inversely from water retention data using the model of Cihan et al. (2007). In developing models for the Menger sponge, we assumed that the pore shape factor, C, was constant. In reality, C can be highly variable in natural porous media and clearly there is no single C value; however, equivalent C values for possible pore shapes can be estimated from numerical simulations performed on scanned soil images.

The analytical model predictions compared favorably with the lattice Boltzmann simulations for the intrinsic

TABLE 4. Comparison of the results for intrinsic permeability (k) from the lattice Boltzmann method (LBM) and the Marshall's probabilistic approach (MPA) models for the random Menger sponge.

Iteration	Porosity, ϕ_3	Effective porosity, $\phi_{eff\,3}$	Measure of connectivity, P	k (MPA)	k (LBM)
				—— × 10^{-4} cm² ——	
3	0.59	0.23 (mean)	0.21 (mean)	3.27	2.57 (mean)
		0.22 (mode)	0.20 (mode)		2.35 (mode)

permeability of both deterministic and random Menger sponges of a 1-cm width, with $b = 3$, $n = 3$, and $D = 2.726\ldots$. The results showed that the intrinsic permeability of the random structure is less than that of the deterministic ones. The modal LBM permeability of 100 realizations of the random Menger sponge was 54% lower than the permeability of the deterministic Menger sponge. A similar trend was observed for the analytical models going from the deterministic to the random structure. Further research is needed to verify the models both with numerical simulations on artificial porous media with scaling factors other than $b = 3$ and with experiments on natural porous media for which fractal parameters can be measured independently.

One might also extend the probabilistic and fractal approaches presented here to the derivation of relative permeability models for the case of unsaturated flow. Testing of new analytical models is achievable with a multiphase lattice Boltzmann method (Huang et al., 2007) that is free of many of the assumptions commonly made when applying capillary theory to porous media.

Appendix

a	Correction factor in Eq. [1]
b	Scaling factor
C	Pore shape factor
d_i	Side length of pore at iteration level i
D_E	Fractal dimension for an embedding space E
E	Embedding space dimension
h	Potential energy per unit volume
i	Iteration level
j	Index variable for summation or product symbols
k	Intrinsic permeability
n	The last iteration level of the fractal porous medium
n_b	Number of boxes (solid or pore) in each slice of the Menger sponge
n_p	Number of pores in the generator
N_{pE}	Number of pore elements in an embedding space E
N_{sE}	Number of solid elements in an embedding space E
p_i	Probability of finding various sized pores in iteration level i
P	Measure of connectivity
r_i	Pore size at iteration level i
r_1	Maximum pore size
r_0	Characteristic size of a porous medium that shows fractal behavior
x_1	Number of solid elements on a random slice of the Menger sponge
ϕ_E	Porosity in an embedding space E
$\phi_{\text{eff } E}$	Effective porosity in an embedding space E
ψ	Pressure

References

Adler, P.M., and J.F. Thovert. 1993. Fractal porous media. Transp. Porous Media 13:41–78.

Brakensiek, D.L., and W.J. Rawls. 1992. Comment on "Fractal processes in soil water retention" by Scott W. Tyler and Stephen W. Wheatcraft. Water Resour. Res. 28:601–602.

Cihan, A., E. Perfect, and J.S. Tyner. 2007. Water retention models for scale-variant and scale-invariant drainage of mass prefractal porous media. Vadose Zone J. 6:786–792.

Filgueira, R.R., L.L. Fournier, C.I. Cerisola, P. Gelati, and M.G. García. 2006. Particle-size distribution in soils: A critical study of the fractal model validation. Geoderma 134:327–334.

Garrison, J.R., Jr., W.C. Pearn, and D.U. von Rosenberg. 1992. The fractal Menger Sponge and Sierpinski Carpet as models for reservoir rock/pore systems: I. Theory and image analysis of Sierpinski Carpets. In Situ 16: 351–406.

Garza-López, R.A., L. Naya, and J.J. Kozak. 2000. Tortuosity factor for permeant flow through a fractal solid. J. Chem. Phys. 112:9956–9960.

Gibson, J.R., H. Lin, and M.A. Bruns. 2006. A comparison of fractal analytical methods on 2- and 3-dimensional computed tomographic scans of soil aggregates. Geoderma 134:335–348.

Gimenez, D., E. Perfect, W.J. Rawls, and Y. Pachepsky. 1997. Fractal models for predicting soil hydraulic properties: A review. Eng. Geol. 48:161–183.

Hillel, D. 1998. Environmental soil physics. Academic Press, San Diego.

Huang, H., D.T. Thorne, M.G. Schaap, and M.C. Sukop. 2007. Proposed approximation for contact angles in Shan- and Chen-type multi-component multiphase lattice Boltzmann models. Phys. Rev. E 76:066701, doi:10.1103/PhysRevE.76.066701.

Hunt, A.G. 2001. Application of percolation theory to porous media with distributed local conductances. Adv. Water Resour. 24:279–308.

Jacquin, C.G., and P.M. Adler. 1987. Fractal porous media: II. Geometry of porous geological structures. Transp. Porous Media 2:571–596.

Kirihara, S., M.W. Takeda, K. Sakoda, K. Honda, and Y. Miyamoto. 2006. Strong localization of microwave in photonic fractals with Menger-sponge structure. J. Eur. Ceramic Soc. 26:1861–1864.

Mandelbrot, B.B. 1982. The fractal geometry of nature. W.H. Freeman, New York.

Marshall, T.J. 1958. A relation between permeability and size distribution of pores. J. Soil Sci. 9:1–8.

Mayama, H., and K. Tsujii. 2006. Menger sponge-like fractal body created by a novel template method. J. Chem. Phys. 125:124706, doi:10.1063/1.2336200.

Millington, R.J., and J.P. Quirk. 1961. Permeability of porous solids. Trans. Faraday Soc. 57:1200–1206.

Muller, J., and J.L. McCauley. 1992. Implication of fractal geometry for fluid flow properties of sedimentary rocks. Transp. Porous Media 8:133–147.

Pan, C., L.-S. Luo, and C.T. Miller. 2006. An evaluation of lattice Boltzmann schemes for porous medium flow simulation. Comput. Fluids 35:898–909.

Papanastasiou, T.C., G.C. Georgiou, and A.N. Alexandrou. 2000. Viscous fluid flow. CRC Press, Boca Raton, FL.

Rawls, W.J., D.L. Brakensiek, and S.D. Logsdon. 1993. Predicting saturated hydraulic conductivity utilizing fractal principles. Soil Sci. Soc. Am. J. 57:1193–1197.

Succi, S. 2001. The lattice Boltzmann equation for fluid dynamics and beyond. Clarendon Press, Oxford, UK.

Sukop, M.C., E. Perfect, and N.R.A. Bird. 2001. Impact of homogeneous and heterogeneous algorithms on water retention in simulated prefractal porous media. Water Resour. Res. 37:2631–2636.

Sukop, M.C., and D.T. Thorne, Jr. 2006. Lattice Boltzmann modeling: An introduction for geoscientists and engineers. Springer-Verlag, Berlin.

Wolf-Gladrow, D.A. 2000. Lattice-gas cellular automata and lattice Boltzmann models: An introduction. Springer-Verlag, Berlin.

Xu, P., and B. Yu. 2008. Developing a new form of permeability and Kozeny–Carman constant for homogeneous porous media by means of fractal geometry. Adv. Water Resour. 31:74–81.

Xu, P., B. Yu, Y. Feng, and Y. Liu. 2006a. Analysis of permeability for the fractal-like tree network by parallel and series models. Physica A 369:884–894.

Xu, P., B. Yu, Y. Feng, and M. Zou. 2006b. Permeability of the fractal disk-shaped branched network with tortuosity effect. Phys. Fluids 18:078103, doi:10.1063/1.2221861.

Yu, B., and W. Liu. 2004. Fractal analysis of permeabilities for porous media. AIChE J. 50:46–57.